APOE gene-dependent BOLD responses to a breath-hold across the adult lifespan

Peter M. Rasmussen[a,*], Rasmus Aamand[a], Eddie Weitzberg[b], Michael Christiansen[c], Leif Østergaard[a], Torben E. Lund[a]

[a] Center of Functionally Integrative Neuroscience, Department of Clinical Medicine, Aarhus University, Aarhus, Denmark
[b] Department of Physiology and Pharmacology, Karolinska Institutet, Stockholm, Sweden
[c] Department for Congenital Disorders, Statens Serum Institut, Copenhagen, Denmark

ABSTRACT

Age and apolipoprotein E (APOE) e4 genotype are two of the strongest known risk factors for sporadic Alzheimer's disease (AD). Neuroimaging has shown hemodynamic response changes with age, in asymptomatic carriers of the APOE e4 allele, and in AD. In this study, we aimed to characterize and differentiate age- and APOE gene-specific hemodynamic changes to breath-hold and visual stimulation. A further aim was to study whether these responses were modulated by 3-day intake of nitrate, a nitric oxide (NO) source. The study was designed as a randomized, double-blinded, placebo-controlled crossover study, and the study cohort comprised 41 APOE e4 carriers (e3/e4 or e4/e4 genotype) and 40 non-carriers (e3/e3 genotype) aged 30–70 years at enrollment. The participants underwent two scanning sessions, each preceded by ingestion of sodium nitrate or sodium chloride (control). During functional magnetic resonance imaging (fMRI) sessions, participants performed two concurrent tasks; a breath-hold task to probe cerebrovascular reactivity and a visual stimulation task to evoke functional hyperemia, respectively. We found that the blood oxygenation level dependent (BOLD) hemodynamic response to breath-hold was altered in APOE e4 carriers relative to non-carriers. Mid-aged (50–60 years of age) e4 carriers exhibited a significantly increased peak time relative to mid-aged e3 carriers, and peak time for younger (30–40 years of age) e4 carriers was significantly shorter than that of mid-aged e4 carriers. The response width was significantly increased for e4 carriers. The response peak magnitude significantly decreased with age. For the visual stimulation task, we found age-related changes, with reduced response magnitude with age but no significant effect of APOE allele type. We found no effect of nitrate ingestion on BOLD responses evoked by the breath-hold and visual stimulation tasks. The APOE gene-dependent response to breath-hold may reflect NO-independent differences in vascular function.

1. Introduction

1.1. Strong risk factors for Alzheimer's disease

Alzheimer's disease (AD) is a neurodegenerative disease and the most common cause of dementia. Late-onset, or sporadic, AD is the most common form of the disease, typically affecting subjects over 65 years of age. The strongest known risk factors for sporadic AD are older age, a family history of AD, and the e4 variant of the apolipoprotein E (APOE) gene allele. Of the three APOE gene alleles (e2, e3, and e4), the e3/e3 combination is the most common. Relative to e3/e3 carriers, the risk for developing AD is increased three-fold for subjects with one copy of the e4 allele (e3/e4), and eight to 12-fold for subjects with two copies (e4/e4) (Alzheimer's Association, 2018).

1.2. Cerebrovascular changes in ageing and AD

Although the etiopathogenesis of AD is still incompletely understood, accumulating evidence suggest a link between cerebrovascular dysfunction and AD (de la Torre, 2004; Farkas and Luiten, 2001; Iadecola, 2017; Kisler et al., 2017; Nelson et al., 2016; Østergaard et al., 2013). Cerebral blood vessel undergo structural and functional changes with age (Farkas and Luiten, 2001). Ageing is associated with atherosclerotic changes, microvascular fibrosis, thickening of the microvessel

basement membrane, venous collagenosis, and changes in vessel compliance. Similarly, increased vessel tortuosity, string vessel formation, and reductions of vessel density alter vessel network topology with ageing and in AD. Vascular risk factors, such as hypertension, diabetes, and atherosclerosis, and genetic risk factors, such as APOE e4 genotype, are known to cause to cerebrovascular damage and dysfunction, possibly contributing to the development of AD and dementia (Kisler et al., 2017; Nelson et al., 2016). In particular, the APOE e4 allele has been associated with accelerated pericyte degeneration, blood brain barrier (BBB) damage and breakdown, cerebral amyloid angiopathy, fibrinogen deposition, and reduced clearance of amyloid-β (Aβ) across the BBB (Kisler et al., 2017; Nelson et al., 2016), all of which are features of AD and likely to affect the proper function of the neurovascular unit (NVU). Aβ has vasoactive and toxic effects on cerebral blood vessels, and experimental models have suggested that its accumulation leads to cerebral blood flow (CBF) dysregulation (Niwa et al., 2000). However, studies in experimental models of pericyte-, vascular smooth muscle cell- (VSMC), and endothelial dysfunction suggest that early CBF dysregulation may be *independent* of Aβ (Kisler et al., 2017). Since brain health critically depends on an adequate distribution of blood flow across the cerebral microvasculature (Jespersen and Østergaard, 2012), the vascular changes observed with ageing and with disease development may thus contribute to neuronal dysfunction, neurodegenerative changes, and cognitive loss (Kisler et al., 2017; Nelson et al., 2016; Østergaard et al., 2013).

1.3. Functional neuroimaging changes with age and APOE genotype

Neuroimaging provides the means for studying changes in cerebral hemodynamics and blood oxygenation in normal ageing, in subjects at increased risk of developing AD (e.g. APOE e4 carriers), and in patients with mild cognitive impairment (MCI) or AD. Positron emission tomography (PET) and functional magnetic resonance imaging (fMRI) studies suggest that resting CBF decreases with age (Ances et al., 2009; D'Esposito et al., 2003; Lu et al., 2011; Reich and Rusinek, 1989). Several studies have investigated age-related changes in the blood oxygenation level dependent (BOLD) signal as evoked by visual tasks (Aizenstein et al., 2004; Ances et al., 2009; Buckner et al., 2000; Huettel et al., 2001; Ross et al., 1997; Tekes et al., 2005) and motor tasks (Buckner et al., 2000; D'Esposito et al., 1999; Hesselmann et al., 2001); with reports of age-related declines in observed BOLD responses (Aizenstein et al., 2004; Ances et al., 2009; Buckner et al., 2000; Hesselmann et al., 2001). The generalization of these findings, however, are confounded by changes in signal-to-noise ratios with age (Aizenstein et al., 2004; D'Esposito et al., 1999; Huettel et al., 2001), the use of different voxel selection strategies (Aizenstein et al., 2004; Ances et al., 2009), and an apparent dependence of which brain region and which experimental task is used when studying age-related BOLD response changes (Buckner et al., 2000). Findings of altered CBF or BOLD responses with age invariably begs the question: Do they reflect changes in neuronal processing, altered neurovascular coupling (the change in CBF or BOLD signal for a given amount of neuronal 'work'), or both? Age-related changes in cerebrovascular reactivity (CVR) to chemical modulators of vascular tone have thus been investigated (Ances et al., 2009; Ito et al., 2002; Lu et al., 2011; Peng et al., 2018; Reich and Rusinek, 1989). Widespread decreases in CVR (BOLD response) to CO_2 inhalation with age have been observed (Lu et al., 2011; Peng et al., 2018), and CVR mapping by breath-hold, during which CBF increases as a result of elevated CO_2 levels (Iadecola, 2004), has shown increased delay in BOLD responses and reduced, responding tissue volume with ageing (Raut et al., 2016).

In asymptomatic APOE e4 carriers, resting CBF and CBF responses to functional activation are both augmented relative to control subjects decades before the typical onset of memory symptoms (Fleisher et al., 2009; Scarmeas et al., 2005; Thambisetty et al., 2010). Altered BOLD responses, e.g. elevated BOLD responses to memory tasks (Suri et al.,

2015), have also been observed in young APOE e4 carriers, although the presence and the directionality of BOLD response changes in APOE e4 carriers relative to e3 carriers appear to be considerably influenced by experimental task, subject age, family history of AD, data analysis strategy, and other factors (Trachtenberg et al., 2012). Reduced CVR to CO_2 inhalation has been observed in young APOE e4 carriers by BOLD fMRI (Suri et al., 2015), and in old APOE e4 carriers by transcranial Doppler ultrasonography (Hajjar et al., 2015). In patients diagnosed with amnestic MCI or late-onset AD, CVR to CO_2 inhalation has also been assessed by means of BOLD responses, in both cases showing reduced slope and amplitude of their responses relative to control subjects (Cantin et al., 2011).

1.4. Influence of nitric oxide on cerebral hemodynamics

Nitric oxide (NO) is a strong modulator of CBF (Attwell et al., 2010; Iadecola, 2004; Kisler et al., 2017; Lavi et al., 2003) and an important component of signaling pathways underlying neurovascular coupling mechanisms (Attwell et al., 2010; Iadecola, 2004; Kisler et al., 2017). NO promotes relaxation of VSMCs and inhibits their constriction (Attwell et al., 2010; Iadecola, 2004; Kisler et al., 2017), and NO may also be part of signaling pathways that control capillary blood flow distributions through constriction and relaxation of pericytes (Kisler et al., 2017). NO production is catalyzed by nitric oxide synthases (NOS), and the principal source of NO in the vascular system is endothelial NOS (eNOS) within endothelial cells (de la Torre and Stefano, 2000). Under healthy conditions, basal endothelial NO production maintains a stable cerebral microenvironment by its effect on CBF regulation, by its influence on the morphology of endothelial cells, and by its regulatory effects on immune responses with both blood and tissue (Albrecht et al., 2003; de la Torre and Stefano, 2000; Katusic and Austin, 2014). Meanwhile, disturbances in basal NO production and NO depletion may contribute to a series of potentially harmful changes, e.g. alteration of endothelial cell shape and compensatory thickening of the basement membrane, reduced inhibition of inflammatory responses, increased oxidative stress, remodeling of VSMCs, and abnormal capillary constriction, with concomitant dysregulation of microvascular flow patterns (de la Torre and Stefano, 2000; Østergaard et al., 2013). These events may, in turn, contribute to the progressive development of neurovascular and capillary dysfunction, disturbed energy metabolism, and ultimately to neurodegenerative changes and cognitive decline (de la Torre and Stefano, 2000; Iadecola, 2004; Østergaard et al., 2013).

Administration of exogenous NO, e.g. via sodium nitroprusside (SNP), has a vasodilatory effect and reduces cerebrovascular resistance (Lavi et al., 2003), whereas NOS inhibition has been shown to attenuate CBF responses to hypercapnia in experimental models (Iadecola, 1992) and in humans (Schmetterer et al., 1997). In humans, SNP infusion does not alter resting CBF, but augments the CBF response to CO_2, as measured by the slope of the linear correlation between end-tidal CO_2 and middle cerebral arterial blood velocities measured by Doppler ultrasonography in younger subjects (Lavi et al., 2003). This index of CO_2 vasoreactivity has been shown to be reduced in middle-aged patients with cardiovascular risk factors (diabetes and/or hypertension) relative to age-matched control subjects, however administration of SNP, interestingly, offset this difference in CO_2 vasoreactivity relative to control subjects (Lavi et al., 2006).

The nitrate-nitrite-NO pathway provides an alternative pathway for NO production in the human body (Lundberg et al., 2008). Dietary nitrate may have beneficial vascular effects by reducing blood pressure, by inhibiting inflammatory processes, and by enhancing endothelial function (Bondonno et al., 2016; Lidder and Webb, 2013; Stanaway et al., 2017). In young adults, a period of 3 days with elevated dietary intake has been shown to reduce the delay and magnitude of BOLD responses to visual stimulation (Aamand et al., 2013) and to modulate the temporal dynamics of total-hemoglobin changes measured by near-infrared spectroscopy during cognitive tasks (Wightman et al., 2015). In

older adults, a nitrite-rich diet has been shown to increase CBF in frontal white matter (Presley et al., 2011).

1.5. Study outline

In the present study, we investigated BOLD signal responses to both functional activation and to breath-hold in APOE e3 and e4 carriers. Participant ages spanned four decades (mid-thirties to mid-seventies), and they were each examined twice, each time preceded by either NaCl (sodium chloride, control condition) or $NaNO_3$ (sodium nitrate, treatment condition) ingestion to modulate their endogenous NO levels. Participants performed two concurrent tasks while BOLD responses were being recorded during a fMRI scanning session; a breath-hold task to probe cerebrovascular reactivity (to the concomitant CO_2 and O_2 changes) and a visual stimulation task to evoke functional hyperemia (via neurovascular coupling mechanisms), respectively. The experimental paradigm and the MR acquisition were designed to allow for a representation of the dynamics of the BOLD signal with good temporal resolution. To study hemodynamic response differences according to age, participants were partitioned into sub-groups based on their age. The primary aims of the study were i) to characterize age- and gene-specific hemodynamic responses and their differences, and ii) to study whether these responses were modulated by the elevated nitrate levels resulting from the 3-day ingestion period.

2. Material and methods

2.1. Participants

283 healthy participants were recruited from the general public through advertisements in a local newspaper. Participants were required to be between 30 and 70 years of age at the time of enrolment and have Danish as their main language to ensure understanding of MR safety instructions. Exclusion criteria were prior psychiatric disorder, use of prescription medicine, prior severe allergic reactions, obesity, pregnancy, claustrophobia, reduced kidney function, anxiety (needles, blood), and implants that might interfere with the MR scans. The participants underwent genetic screening to establish their APOE allele status, and 52 carriers of at least one APOE e4 allele (38 e3/e4 and 14 e4/e4 – referred to as APOE e4 carriers) and 48 carriers of two APOE e3 alleles (non-carriers) were retained in the study. These specific participants were selected among the initial study cohort to roughly balance APOE status (APOE e4 carriers/non-carriers), gender, and the distribution of ages across the decades spanning the thirties to the seventies. The study was approved by the Ethics Committee of the Central Denmark Region (1-10-72-239-13) and conducted in accordance with the Helsinki Declaration. All participants gave written informed consent prior to their participation.

2.2. Study design

The study was designed as a randomized, double-blinded, placebo-controlled crossover study, in which participants underwent two scanning sessions. Prior to each scanning session, the participants ingested either sodium chloride (NaCl) or sodium nitrate ($NaNO_3$) over an ingestion period of 3 days. The NaCl and $NaNO_3$ salts were administered as saline solutions mixed with concentrated fruit juice to disguise taste differences. Saline content was 0.1 mmol per kg bodyweight per day. During the ingestion periods, the participants were instructed to avoid the intake of specific vegetables rich in nitrate and instead provided with suggestions for food alternatives in order to reduce interference with the study treatment. Following the first ingestion period, participants underwent the first scanning session. The second ingestion period was separated from the first scanning session by a washout period of at least 10 days. During the second ingestion period, participants ingested the opposite treatment of the first, and the ingestion period was

followed by the second scanning session. Ingestion order was randomized across subjects.

2.3. Acquisition protocol

Scanning was carried out at the Center of Functionally Integrative Neuroscience, Department of Clinical Medicine, Aarhus University, Denmark. The experimental paradigm and the acquisition of fMRI scans and auxiliary physiological measurements were as follows:
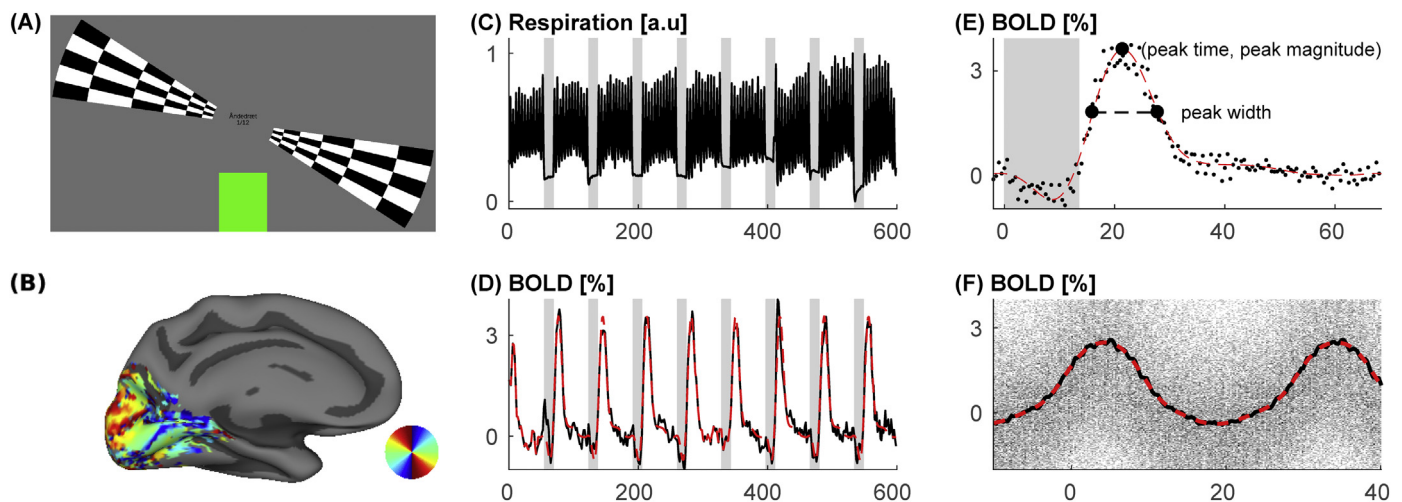
2.3.1. Experimental paradigm

The fMRI scanning session lasted 10 min and involved two concurrent tasks – a breath-hold task and a visual stimulation task. The breath-hold task comprised eight epochs of paced breathing (55 s), expiration and breath-hold (13.5 s) followed by a final period of paced breathing (52 s). In the first scanning session, prior to the start of the experimental paradigm, each participant's natural, resting breathing rate was measured with the participant positioned in supine position in the MR scanner. The breath-hold stimulation paradigm was then constructed according to this measured breathing rate under the constraint of an integer number of breaths during breathing periods to ensure expiration before breath-hold periods. Hence, the participants' breathing rates were paced during both scanning sessions, and the breath-pacing rate was maintained from the first to the second scanning session to ensure identical breath-hold tasks across the two sessions. Breathing was paced visually by varying the height of a vertical bar (Fig. 1A). The height of the bar was set to change in cycles according to the individual breathing rates, and participants were instructed to inhale as bar height increased, and exhale as the bar height decreased. Breath-hold was indicated by a fixed bar height throughout the prescribed duration. Via digits presented in the center of the screen, participants were informed of breath count while breathing and of the time remaining (in seconds) during breath-hold periods. The visual stimulation task consisted of a rotating double wedge stimulus with black/white flickering checkerboard pattern (Fig. 1A). The wedge angle was 25° and the double wedge rotated with a period of 60 s. During the first part of the paradigm, the double wedge rotated clockwise for 285 s, followed by a 30 s break with no wedge stimulation. Finally, the double wedge rotated counterclockwise for 285 s. Participants were instructed to breathe at a comfortable depth and to keep their eyes focused on the text presented in the center of the screen rather than on the double wedge or the vertical breath-pacing bar.

2.3.2. MRI acquisition

MRI was performed on a Siemens Magnetom Skyra 3T system (Erlangen, Germany). In the first scanning session, high-resolution T1-weighted images were acquired for anatomical reference (anatomical scan) with acquisition parameters: MP2RAGE sequence, 1 mm isotropic voxels, matrix size = 240 × 256 × 176, repetition time (TR) = 5000 ms, echo time (TE) = 2.98 ms, inversion time (TI) = 700 ms & 2500 ms, flip angle (FA) = 4° & 5°, and GRAPPA using an iPAT factor of 2. Functional scans were acquired in both scanning sessions with acquisition parameters: Gradient echo (GE) echo planar imaging (EPI) sequence, 3 mm isotropic voxels, matrix size = 64 × 64 × 29, TR = 1500 ms, TE = 27 ms, FA = 60° and GRAPPA using an iPAT factor of 3.

2.3.3. Blood samples

APOE genotype was determined at Statens Serum Institut, Copenhagen, Denmark. Blood samples, used to determine plasma levels of nitrate and nitrite, were collected before each ingestion period and immediately before and after each scanning session. Plasma content of nitrate and nitrite was determined at Department of Physiology and Pharmacology, Section of Anesthesiology and Intensive Care, Karolinska Institutet, Stockholm, Sweden. The nitrate and nitrite levels before and after individual scanning sessions were averaged.

Fig. 1. Conceptual fig. (A) Experimental paradigm with two concurrent tasks – a breath-hold task and a visual stimulation task. Breathing was controlled by changes in the height of the vertical bar. Bar height changed in cycles during periods with paced breathing and remained constant during breath-hold periods. Visual stimuli was delivered by means of a rotating double wedge with a flickering checkerboard pattern. (B) Surface-based representation of a phase map estimated from BOLD responses evoked by the visual stimulation task. (C) Respiratory recordings illustrating the breath-hold task. Gray shaded areas mark breath-hold periods. (D) Average gray matter BOLD response (black curve) evoked by the breath-hold task and cosine expansion model fit (dashed red curve). (E) Average BOLD responses to breath-hold responses (black dots) and cosine expansion fit (dashed red curve). The response was represented by three hemodynamic features: peak time, peak magnitude, and peak width. (F) BOLD response to visual stimulation. Individual voxels' responses were time shifted according to phase estimates (B) and a delay parameter. Gray shades indicate density estimates of point scatter of the time shifted responses, the black curve show time-binned response estimates, and the dashed red curve shows a cosine expansion model fit to the response estimate. Unit of abscissae in C−F is seconds.

2.3.4. Auxiliary physiological recordings

Blood pressure was measured using a Medrad® Veris® MR Vital Signs Monitor (Warrendale, USA). Recordings of respiration, heart rate, oxygen saturation, and transcutaneous CO_2, were continuously acquired during the scanning sessions. Respiratory recordings were acquired using the scanner's pneumatic belt, which was connected to a custom built pressure sensor which did not saturate during deep breaths. Heart rate, oxygen saturation, and CO_2 were recorded using a transcutaneous Sentec V-Sign® sensor, (SENTEC-AG, Therwil, Switzerland) connected to a Brain Vision BrainAmp ExG MR amplifier (Gilching, Germany). The transcutaneous sensor was attached to the participant's cheek by an attachment ring placed just below the right eye, where skin is thin, allowing these recordings to serve as a proxy of blood CO_2. Further details on the CO_2 measurement setup is available in Supplementary Fig. S1.

2.4. Data processing and quantification

2.4.1. MRI data pre-processing

MRI data was processed in Matlab using the SPM12 (www.fil.ion.ucl.ac.uk/spm/) and CAT12 (www.neuro.uni-jena.de/cat/) software packages. Spatial coordinates of the anterior commissure were interactively identified from anatomical scans and these coordinates were used to re-reference the origin of anatomical and functional scans. Anatomical scans were further processed using the CAT12 toolbox, which yielded a series of tissue probability maps, transformations between subject space and MNI space, and a triangular representation of the cortical surface.

Tissue probability maps were used to isolate brain voxels and to define subject specific tissue ROIs. First, brain voxels were defined by the set of voxels where the sum of probabilities inferred from GM, WM, and CSF probability maps was > 0.5 ensuring that brain tissue was the most probable (≥50%) tissue class for these voxels. A GM mask was then defined by voxels for which the GM probability was higher than that of belonging to either WM and CSF. A set of eight anatomical ROIs – frontal, parietal, occipital, temporal, thalamus, cingulate, striatum, and insula – were further defined by first mapping the AAL atlas in SPM to subject space and then combining individual atlas regions to yield

these eight overall ROIs (Cantin et al., 2011). Similarly, another set of seven ROIs were defined from the resting state network atlas provided with the CONN toolbox (Whitfield-Gabrieli and Nieto-Castanon, 2012). Cerebellar voxels were excluded from the analyses because of incomplete scan coverage.

Functional scans were slice-time corrected and motion corrected using session means as references. The second session functional mean was co-registered to the first session functional mean and the resulting transformation was applied to all functional scans of the second session. The functional means of the two sessions were then co-registered to the anatomical scan, and the transformations were applied to all functional scans of the individual sessions. Finally, the co-registered functional scans were resliced to 3 mm isotropic voxels.

Low-frequency components of the functional time series were removed by projecting out fits to a discrete cosine transform basis set with a cut-off period of 128 s. Paced breathing may result in breathing-related signal variations that appear systematically across epochs. These signal variations were filtered out by modeling, at the voxel-level, the respiratory effects by a basis set of sines and cosines (RETROICOR) (Glover et al., 2000; Lund et al., 2006). The basis set was constructed from the respiratory recordings and comprised basis functions up to the second harmonic. Elements in the respiratory regressors corresponding to breath-hold periods were effectively disregarded by modeling these time points by scan nulling regressors. Finally, the fits to the respiratory regressors were regressed out of the fMRI data.

2.4.2. Functional time series quantification and modeling

Voxel-wise baseline values were estimated by averaging scans across the final ten seconds of the breath-pacing periods across all epochs, and voxel time series were then converted into percent changes by normalizing them by the baseline estimates.

Signal responses evoked by the breath-hold task and the visual stimulation task were modeled in a single general linear model (GLM). The breath-hold task was modeled by sine and cosine regressors at the task frequency (f = 1/68.5 Hz) and harmonics up to 5th order. The visual stimulation task was modeled by sine and cosine regressors at half the task frequency (f = 1/30 Hz, because of the 30 s between individual wedges) to facilitate the analytical estimation of voxel-specific

response phases and delays (Thirion et al., 2006) (Fig. 1B). These phases and delays were then used to obtain an average visual stimuli response curve by shifting individual voxel's time series according to the phase and delay estimates (details below).

Scan-nulling regressors were added to the GLM to effectively remove contributions from (i) the first 45 s of acquisition, (ii) scans acquired during the visual stimulus break and during the first visual task period after the break (time 285 s–345 s), (iii) scans, which belonged to breath-hold periods and subsequent paced breathing periods that had to be rejected because the subject failed to follow on-screen instructions. These rejections were based on visual inspection of respiratory time series, Fig. 1C. Rejection criteria were (i) irregular breathing during periods with paced breathing, (ii) failure to exhale before breath-hold periods, and (iii) breathing during breath-hold periods.

Fitted time courses of the breath-hold regressors were averaged over ROI voxels, Fig. 1D. Only GM voxels were considered and the analysis was further confined to only include voxel surpassing a goodness-of-fit metric (r^2) of 0.1. A series of response features were extracted to parameterize the resulting response curve - peak time (relative to breath-hold start), peak magnitude, and peak width quantified by the full with half maximum (FWHM), Fig. 1E.

Fitted coefficients corresponding to the visual task sine and cosine regressors were used to calculate voxel-wise magnitudes and the phases of the fitted responses (cosines) for the forward and reverse visual stimulation round. A hemodynamic delay parameter, which can be calculated from the estimated phases of the forward and reverse stimulation round (Thirion et al., 2006), was further calculated. The cosine magnitude and the delay features were then averaged across ROI voxels. Only GM voxels within the occipital ROI were considered, and the analysis was further confined to only include voxel surpassing a goodness-of-fit metric (r^2) of 0.1. The estimated phases and delays were further used to extract a more detailed response curve. Time axes, one for each voxel, were time shifted according to the estimated phases and delays to temporally align individual voxels' time series (different voxels stimulated at different times during the visual stimuli cycle, Fig. 1A,B). The time-shifted time axes were then used to average across included ROI voxels by time binning (bin width 1 s, bin shift 0.25 s), Fig. 1F. Finally, a visual task GLM with sine and cosine regressors at the visual task frequency and harmonics up to 5th order was fitted to the average response and three additional features were extracted: peak time (relative to time zero), peak magnitude, and peak width (FWHM).

2.5. Statistical analysis

Statistical analysis was conducted in R (Team, R.D.C., 2010). The experimental data was organized according to a factorial structure AGE x APOE x NaCl/NaNO$_3$, with AGE being a between-subject factor with levels 30–40, 40–50, 50–60, 60 + years of age, APOE being a between-subject factor with levels e3, e4, and NaCl/NaNO$_3$ being a within-subject factor with levels NaCl and NaNO$_3$. Statistical relationships between these experimental factors and dependent variables/hemodynamic response features were primarily modeled by linear mixed models (R package lme4) (Bates et al., 2015), whereas Poisson regression was used to model the number of paced breaths because of the discrete nature of this response variable. Average CO$_2$, sex, and session, were included as covariates in the models of hemodynamic response features (Cohen et al., 2002; Hesselmann et al., 2001; Stefanovic et al., 2006). Statistical significance was determined from *p*-values, and *p* = .05 was used as significance threshold. Step-wise model reduction was used for reduction of initial models comprising all experimental factors, their interactions, and the covariates (R package lmerTest) (Kuznetsova et al., 2017). A standard approach was used for iterative model selection, in which model comparison (large vs. reduced model) was based on likelihood ratio tests, degrees of freedom were estimated using the Kenward-Rogers technique, and a threshold of 0.1 was used in the iterative selection (Halekoh and Højsgaard, 2014; Kuznetsova et al.,

2017). Estimated marginal means were computed for all factor level combinations and pairwise comparisons among these were conducted by comparing across levels of a single experimental factor for fixed levels of the remaining experimental factors. Adjustment for multiple comparisons was performed by use of Tukey's honest significance test (R package emmeans).

3. Results

We first present result from analysis of subject demographics and macroscopic physiological variable. This analysis was conducted to examine whether systematic differences in these variables were present across the participant groups (age groups, APOE groups) and to evaluate the effect of nitrate ingestion on the macroscopic physiological variables. This analysis is followed by a reproducibility analysis of the hemodynamic response features to assess the feature reliability and stability. We then present our main analysis: the analysis of the breath-hold evoked BOLD responses and visual stimuli evoked BOLD responses.

3.1. Subject demographics and macroscopic physiological variables

3.1.1. Subject exclusion

The size of initial study cohort of 100 participants was reduced because of participant dropout (five participants) and image problems prohibiting successful preprocessing (tissue segmentation, one participant). Furthermore, 13 participants were excluded because of lack of compliance with the breath-hold instructions as judged by visual inspection of the respiratory traces. Seven participants consistently inspired before the breath-hold period but otherwise complied well with the experimental instructions (paced breathing and breath-holding), whereas the remaining six participants exhibited either inspiration before breath-hold, irregular breathing patterns during periods of paced breathing, or breathing during breath-hold periods. Of these 13 participants, one participant belonged to the 30–40 age group, three participants belonged to the 40–50 age group, three participants belonged to the 50–60 age group, and six participants belonged to the > 60 age group. Furthermore, NaCl/NaNO$_3$ intake was incorrect in four participants as judged by nitrate measurements (NaCl/NaNO$_3$ ingestion order swapped in a single participant, two participants ingested NaCl twice, one participant ingested NaNO$_3$ twice). Data from these four participants were included in the analysis following correct assignment of the NaCl/NaNO$_3$ factor in the statistical models. Accordingly, 81 participants in total were retained for further analysis.

3.1.2. Brain characteristics and physiological variables

Table 1 summarizes subject participant demographics. Participants in the 30–40 age group were significantly taller than participants in the 40–50, 50–60, and 60 + age groups (*p* = .028, .033, and .00023, respectively). Males were significantly taller than females (*p* = 1.7E-13) and also weighed more (*p* < .0015). No significant differences in weight or body mass index (BMI) were observed across the age groups. No differences in height, weight, and BMI were found across the APOE groups. Males had larger total intra cranial volumes (TIV) than females (*p* = 1.4E-5). No significant association between total intracranial volume and APOE type was observed. The GM volume fraction decreased significantly with age between the 30–40 age group and the 50–60, and 60 + age groups (*p* = .00040, and 5.0E-8, respectively), and between the 40–50 age group and the 50–60, and 60 + age groups (*p* = .0065, and 3.3E-6, respectively). The CSF volume fraction, in turn, increased significantly with age between the 30–40 age group and the 50–60, and 60 + age groups (*p* = .0038, and 1.6E-8, respectively), between the 40–50 age group and the 50–60, and 60 + age groups (*p* = .025, and 3.0E-7, respectively), and between the 50–60 age group and the 60 + age group (*p* = .0056). The WM volume fraction showed no significant association with age. No significant associations between the tissue

Table 1
Participant demographics, brain volumes, and respiratory frequency as grouped by age group and APOE allele type.

Age group	APOE	Age [years]	Subjects (females)	Height [cm]*§	Weight [kg]§	BMI [kg/m²]	Resp. freq. [1/min]	TIV [ml]§	GM rel. Vol. [%]*	WM rel. Vol. [%]	CSF rel. Vol. [%]*
30–40	e3	35.7 (2.7)	10 (3)	180 (7)	77 (12)	24 (2)	14 (2)	1586 (199)	48 (3)	34 (2)	18 (3)
	e4	34.5 (2.0)	8 (3)	180 (7)	79 (9)	25 (3)	13 (2)	1659 (217)	48 (3)	35 (1)	17 (2)
40–50	e3	46.1 (1.4)	8 (6)	168 (9)	75 (18)	26 (5)	14 (3)	1482 (184)	47 (2)	34 (1)	19 (3)
	e4	46.4 (3.0)	9 (6)	170 (11)	75 (14)	26 (4)	12 (3)	1470 (149)	49 (2)	34 (1)	18 (3)
50–60	e3	55.3 (3.3)	11 (6)	173 (9)	76 (14)	25 (4)	13 (3)	1525 (192)	45 (2)	35 (2)	20 (3)
	e4	56.8 (2.4)	12 (7)	171 (12)	75 (21)	25 (6)	13 (3)	1487 (126)	45 (3)	34 (2)	21 (3)
60+	e3	65.2 (2.2)	11 (5)	170 (5)	77 (11)	27 (5)	13 (3)	1583 (130)	44 (2)	33 (2)	23 (3)
	e4	65.7 (3.3)	12 (5)	171 (7)	70 (11)	24 (2)	13 (2)	1525 (166)	44 (2)	33 (2)	23 (2)

Abbreviations: APOE, apolipoprotein E; BMI, body mass index; TIV, total intracranial volume; GM, gray matter; WM, white matter; CSF, cerebrospinal fluid. Format: mean (standard deviation). Symbols denote presence of significant between-group differences with respect to age(*), APOE(†), nitrate treatment(‡) and gender(§), respectively. See Section 3.1.2. for detailed description of between-group differences.

volume fractions and APOE type were observed. No significant differences in respiratory frequencies (paced respirations) were observed across the age and APOE sub-groups.

Table 2 summarizes physiological variables. $NaNO_3$ intake significantly increased plasma nitrate concentration ($p = 2.2E\text{-}16$) and plasma nitrite concentration ($p = 5.4E\text{-}4$), Fig. 2A,B. Age groups and APOE type showed no statistically significant influence on plasma nitrate and nitrite concentrations. A single subject was left out from nitrate/nitrite analysis because of high nitrite measurement ($> 3\,\mu M$), which resulted in significant higher order model interaction terms that totally disappeared when this subject was left out. Average oxygen saturation recordings and average CO_2 recordings both increased significantly from first to second session ($p = .018$, and 8.0E-10, respectively), whereas heart rate significantly decreased from first to second session ($p = .0029$). No significant differences in average oxygen saturation recordings, average CO_2 recordings, or heart rate, were observed across the age groups, the APOE types, and the $NaCl/NaNO_3$ treatments. Across all participants we observed a slow drift in CO_2 recordings during the scanning sessions as previously reported (Murphy et al., 2011). The temporal response characteristics of the CO_2 sensor did not allow for a robust characterization of changes in CO_2 levels evoked by individual breath-hold epochs. Hence, only average CO_2 levels were considered in subsequent analyses (see discussion). Systolic blood pressure decreased significantly after nitrate intake ($NaNO_3$ session, $p = .015$) and increased significantly with age between the 30–40 age group and the 60+ age group ($p = .019$), and between the 40–50 age group and the 60+ age group ($p = .018$). Diastolic blood pressure increased significantly with age between the 30–40 age group and the 60+ age group ($p = .0012$). Mean blood pressure increased significantly between the 30–40 age group and and 60+ age group ($p = .0026$) and between the 40–50 age group and the 60+ age group ($p = .029$). Additionally, systolic-, diastolic-, and mean blood pressure all decreased from the first to the second session ($p = 8.5E\text{-}5$, .013, and .0012, respectively).

3.2. Session-wise reproducibility of hemodynamic response features and CO_2 recordings

To evaluate the stability and reliability of response features characterizing the BOLD responses we first quantified the between-session reproducibility of features representing single subject BOLD responses: peak time, peak magnitude, and peak width for the breath-hold task, and cosine delay, cosine magnitude, peak time, peak magnitude, and peak width for the visual stimulation task. Scatter plots that provide a visual representation of feature reproducibility are shown in Fig. 3. A strong between-session reproducibility, as parameterized by between-session correlation, was observed for all response features (VS peak width feature: $p = .0014$, all other features: $p < 1.0E\text{-}10$), and a strong between-session correlation for the average CO_2 recordings ($r = 0.82$, $p = 3.8E\text{-}19$) was also observed.

3.3. Analysis of breath-hold response features

Results from an analysis based on the whole-brain ROI comprising cortical and subcortical gray matter voxels are first presented followed by results from region specific analyses. This is followed by a presentation of group specific response curves, and finally an analysis of the impact of voxels selection threshold on the analysis results.

3.3.1. Dependent variable: peak time

Model reduction lead to a final model with the age-APOE interaction and the CO_2 covariate retained as independent variables (model $p = .01$). Within individual age groups, we observed a significantly increased peak time for APOE e4 carriers in the 50–60 age group (mean difference e3-e4: -1.7 s, $p = .020$), Fig. 4A. Within the two APOE groups, we observed a significant peak time difference within the APOE

Table 2
Physiological variables as grouped by age group, APOE allele type, and NaCl/NaNO$_3$ ingestion.

Age group	APOE	Ingestion	Nitrate [μM] ‡	Nitrite [μM] ‡	CO$_2$ [mmHg]¶	SO$_2$ [mmHg]¶	Heart rate [1/min]¶	BPsys [mmHg]‡,¶,*	BPdia [mmHg]¶,*	BPmbp [mmHg]¶,*
30–40	e3	NaCl	33 (18)	0.6 (0.4)	38 (3)	98 (1)	60 (8)	123 (12)	70 (10)	88 (9)
		NO3	416 (91)	0.7 (0.3)	37 (4)	98 (1)	61 (10)	120 (14)	70 (12)	87 (12)
	e4	NaCl	45 (29)	0.5 (0.3)	38 (3)	98 (1)	58 (12)	126 (16)	69 (12)	88 (12)
		NO3	414 (71)	0.6 (0.3)	38 (5)	98 (1)	58 (14)	126 (12)	73 (7)	90 (8)
40–50	e3	NaCl	29 (11)	0.5 (0.4)	33 (6)	99 (2)	65 (12)	124 (15)	75 (12)	91 (12)
		NO3	373 (90)	0.9 (0.7)	33 (6)	98 (2)	66 (15)	126 (21)	77 (13)	93 (16)
	e4	NaCl	38 (21)	0.5 (0.2)	35 (6)	98 (1)	66 (6)	122 (14)	73 (12)	89 (12)
		NO3	488 (156)	0.7 (0.6)	34 (5)	98 (1)	70 (5)	121 (17)	72 (13)	88 (14)
50–60	e3	NaCl	25 (11)	0.6 (0.4)	36 (5)	98 (1)	63 (9)	133 (10)	82 (9)	99 (9)
		NO3	374 (82)	0.7 (0.3)	37 (5)	98 (1)	62 (6)	124 (16)	76 (10)	92 (12)
	e4	NaCl	28 (8)	0.5 (0.4)	36 (5)	98 (1)	61 (8)	124 (7)	76 (6)	92 (6)
		NO3	429 (147)	0.7 (0.5)	36 (4)	98 (1)	59 (9)	121 (6)	72 (6)	88 (6)
60+	e3	NaCl	28 (4)	0.9 (0.5)	36 (3)	98 (1)	64 (12)	141 (12)	84 (10)	103 (10)
		NO3	458 (78)	1.1 (0.5)	35 (3)	98 (1)	62 (12)	135 (13)	82 (10)	100 (10)
	e4	NaCl	28 (7)	0.6 (0.4)	37 (6)	98 (1)	65 (11)	132 (14)	78 (8)	96 (10)
		NO3	400 (92)	0.7 (0.5)	36 (6)	98 (1)	66 (10)	131 (9)	80 (4)	97 (5)

Abbreviations: APOE, apolipoprotein E; NaCl, sodium chloride; NaNO$_3$, sodium nitrate; CO$_2$, carbon dioxide; SO$_2$, oxygen saturation; BP, blood pressure; sys/dia/mbp, systolic/diastolic/mean blood pressure. Format: mean (standard deviation). Symbols denote presence of significant between-group differences with respect to age(*), APOE(†), nitrate treatment(‡), gender(§) and session(¶), respectively. See Section 3.1.2. for detailed description of between-group differences.
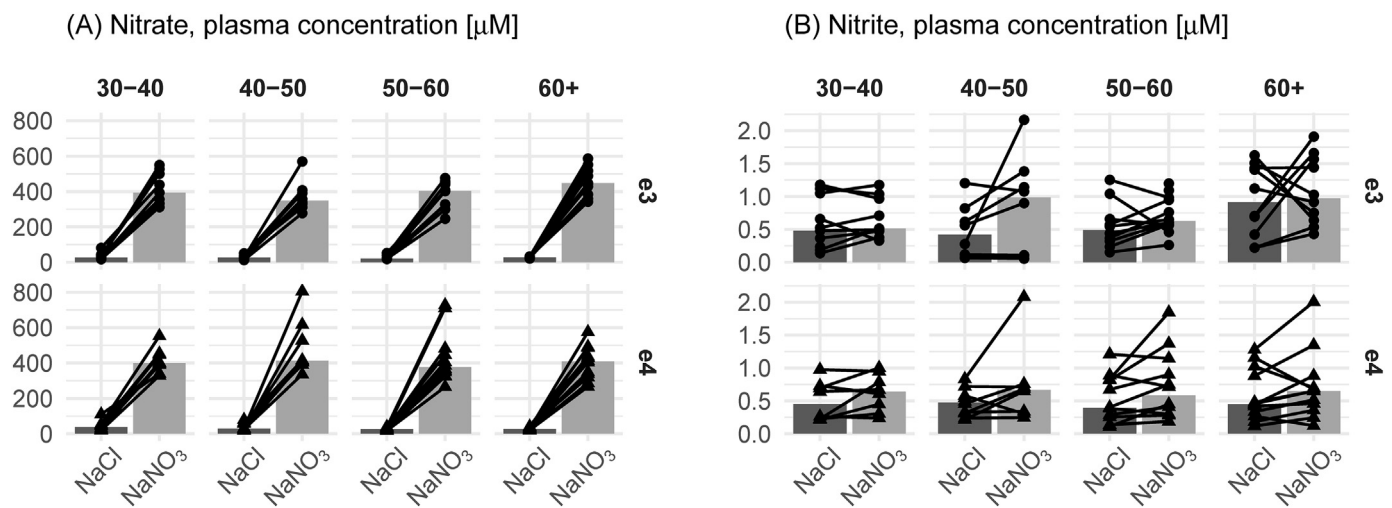
Fig. 2. Plasma concentrations of nitrate (A) and nitrite (B) measured after ingestion periods of 3 days. Ingestion of NaNO$_3$ significantly increased plasma concentration of both nitrate ($p = 2.2E\text{-}16$) and nitrite ($p = 5.4E\text{-}4$). Age groups in columns, and APOE types in rows.

e4 group when comparing the 30–40 and 50–60 age groups (mean difference 30–40 – 50–60: -2.3 s, $p = .021$). Peak time increased significantly with CO$_2$ levels, with a mean effect of 0.11 s/mmHg ($p = .0026$). No significant associations were found between peak time and the treatment factor (NaCl/NaNO$_3$), or the sex and session covariates.

3.3.2. Dependent variable: peak magnitude

Model reduction lead to a final model with the age factor and the CO$_2$ covariate retained as independent variables (model $p = 4.5E\text{-}5$). Peak magnitude decreased significantly with age between the 30–40 age group and the 50–60, and 60 + age groups (mean differences 30–40 - 50–60: 0.54%, $p = .0071$, and 30–40 - 60+: 0.56%, $p = .0052$, respectively), Fig. 4B. Peak magnitude decreased significantly with CO$_2$ level with a mean effect of -0.041%/mmHg ($p = 8.8E\text{-}5$). APOE e4 carriers consistently showed reduced peak magnitude (-0.19%, $p = .11$) although this effect did not reach the criteria for a significant relation, Fig. 4B. No significant associations were found between peak magnitude and the treatment factor or the sex and session covariates.

3.3.3. Dependent variable: peak width

Model reduction lead to a final model with the APOE factor and the CO$_2$ and sex covariates remaining as independent variables (model $p = 3.9E\text{-}5$). APOE e4 carriers had a significantly wider peak than e3 carriers (mean difference e3–e4: -1.4 s, $p = .0080$). Peak width significantly increased with CO$_2$ level with a mean effect of 0.17 s/mmHg ($p = 2.1E\text{-}4$). No significant associations were found between peak width and the treatment factor or the session covariate.

3.3.4. Region specific analyses

Fig. 4D–F provide graphical representations of the analysis conducted in eight anatomical ROIs. Qualitatively, the hemodynamic response features are stable across the individual ROIs in the sense that the ranking of individual subject groups is generally maintained across the eight ROIs. For example, participants in the APOE e4 50–60 subgroup consistently show longer peak times (Fig. 4D) across the ROIs, the largest magnitudes are observed for the APOE e3 30–40 sub-group (Fig. 4E), and the APOE e4 sub-groups had wider responses than the corresponding e3 sub-groups (Fig. 4F). Quantitatively, the numerical values of the response features, the within group scatter, and the resulting presence of statistical significance, differ across the ROIs.
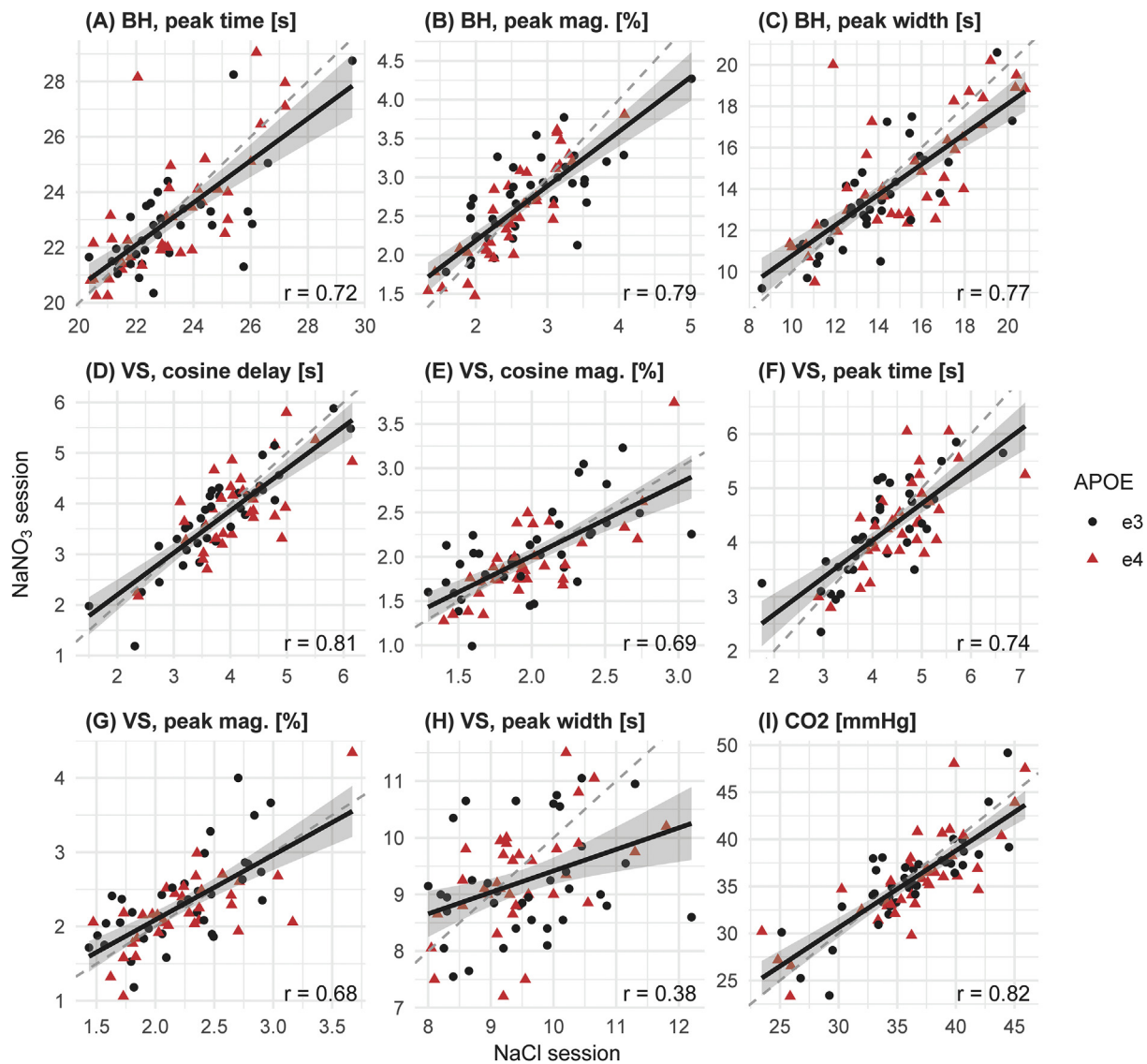
Fig. 3. Reproducibility of hemodynamic response features and average CO2 recordings. Breath-hold (BH) response features were based on a whole-brain ROI comprising cortical and subcortical super-threshold voxels, and visual stimulation (VS) response features were based on super-threshold gray matter voxels in the occipital ROI. Solid lines mark linear fits, shaded regions mark 95% confidence intervals, and the gray dashed lines mark the identity line.

However, the patterns in the statistical significance tests indicate, that the peak time feature primarily captures differences between both age and APOE factor levels, whereas the peak magnitude and the peak width features primarily captures differences between the age and APOE factor levels, respectively. A corresponding analysis conducted in seven resting state network ROIs is available in Supplementary Fig. S2. Similar to the analysis conducted in the anatomical ROIs, the analysis showed effects of age and APOE type on the three hemodynamic response features, also when accumulating data across voxels within the resting state ROIs.

3.3.5. Hemodynamic response curves

Group specific hemodynamic response curves, based on gray matter voxels across the brain, are shown in Fig. 5. Across all participant sub-groups, the breath-hold task evoked a negative dip in the BOLD signal at about 8 s within the breath-hold period, followed by a large magnitude positive peak about 23 s after breath-hold start (and 10 s after breath-hold stop). The positive peak is followed by a period during which the hemodynamic response falls off to baseline. The between-group differences in the average response curves are consistent with the preceding analysis of individual subject hemodynamic response

features. Relative to the APOE e3 sub-group, the APOE e4 sub-group showed shorter peak times within the 30–40 age group, a delayed peak within the 50–60 group, and a similar peak time within the 40–50 and 60 + age groups. Response magnitude decreases with age within both APOE groups. A large decrease in response magnitude between adjacent age group is observed for e4 carriers between the 40–50 and 50–60 age groups. Response curves of the APOE e4 subgroups have smaller peak magnitudes than the corresponding curves of APOE e3 carriers with the largest difference within the 50–60 age group. Within the 40–50 and 50–60 age groups the APOE e3 sub-group exhibit a more rapid and narrow hemodynamic response, whereas the APOE e4 sub-group showed a more dispersed response with delayed peak, lower peak magnitude, and prolonged response tail. ROI specific response curves corresponding to the anatomical ROIs and the resting state network ROIs are available in Supplementary Figs. S3.1–S3.8 and S4.1–S4.7, respectively.

3.3.6. Dependence of voxel selection threshold

To evaluate the impact of the voxel selection threshold (r^2 threshold) on the analysis of breath-hold responses across gray matter voxels (Sections 3.3.1–3.3.4 and Fig. 4A–C), we first evaluated the
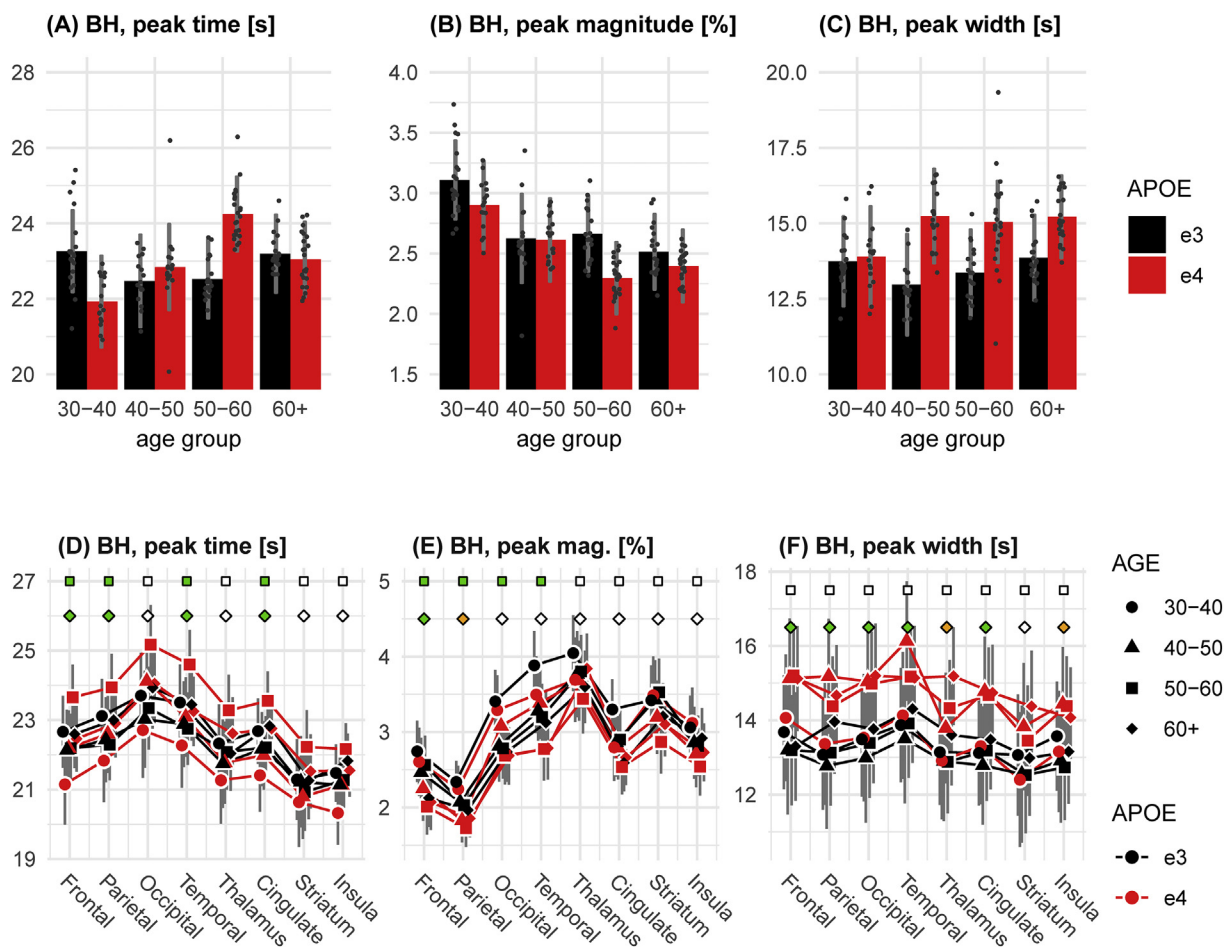
Fig. 4. (A–C) Response features of BOLD responses to breath-hold estimated across gray matter voxels (voxels with $r^2 > 0.1$ included). Bars show estimated marginal means (EMM), gray vertical lines mark 95% confidence intervals, and dots mark individual subjects (EMM plus model error). (A) APOE e4 carriers had significantly longer peak time than e3 carriers in the 50–60 age group, and also significantly longer peak time than e4 carriers in the 30–40 age group. (B) Peak magnitude significantly decreased with age. (C) APOE e4 carriers had significantly wider responses than e3 carriers. See Section 3.3 for detailed description of betweeen-group differences. (D–F) Response features estimated within brain atlas regions (gray matter voxels and voxels with $r^2 > 0.1$ included). The two top rows with squares and diamonds mark the statistical significance of the age group factor (squares) and the APOE type factor (diamonds), whereas green, yellow, and white color denote $p < .05$, $p < .1$, and $p > .1$, respectively (p-values uncorrected across ROIs). Points mark EMMs and gray vertical lines mark 95% confidence intervals.
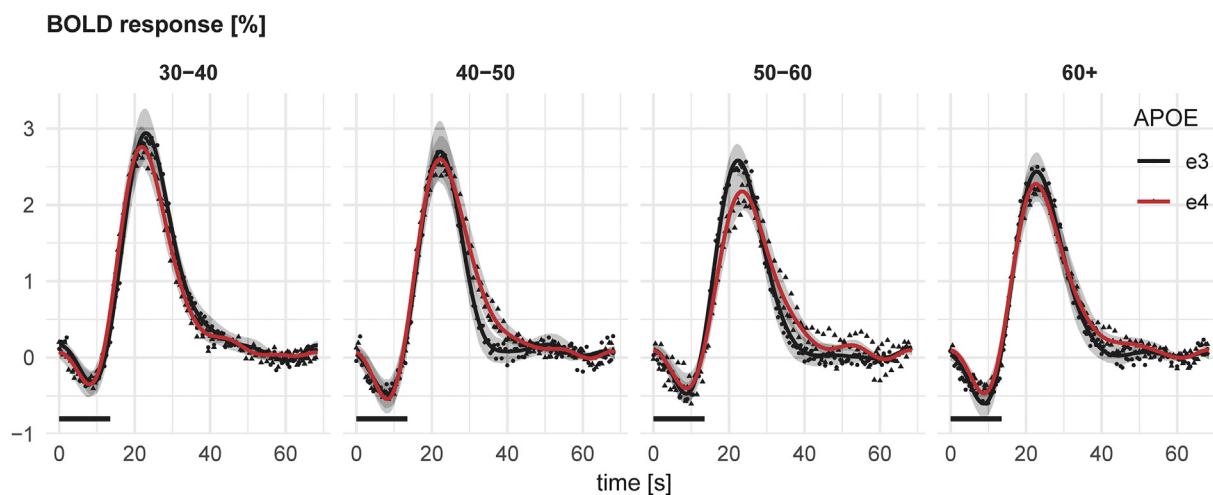
Fig. 5. Group-wise response curves for the breath-hold task. Dots mark average measurements (pooled across all gray matter voxels with $r^2 > 0.1$ and subjects) and curves show average cosine expansion model fits. Gray shaded regions mark 95% confidence intervals of the mean as estimated by bootstrap resampling. Age groups are shown in columns.
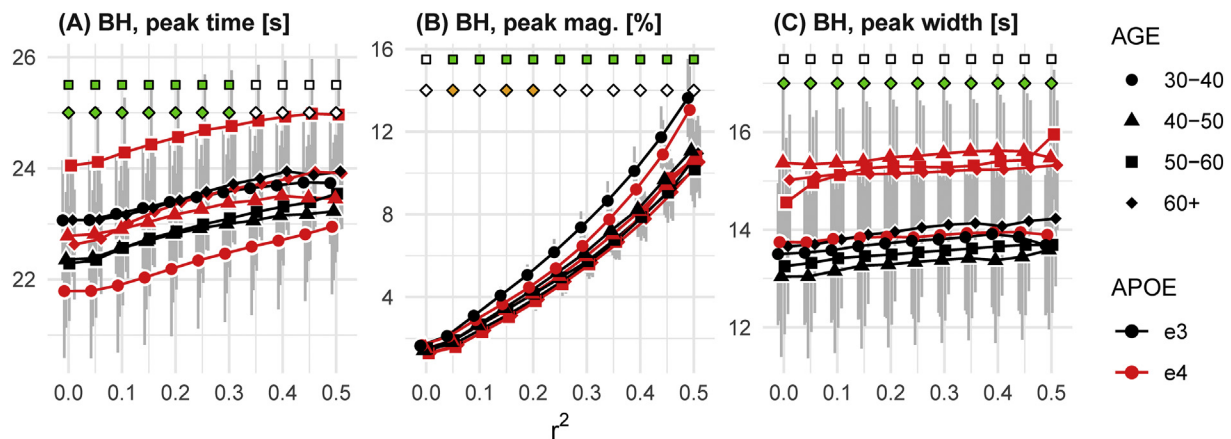
Fig. 6. Dependence of voxel selection threshold (r^2) on breath-hold response features (based on initial ROI containing all gray matter voxels). Same format as Fig. 4(D–F).

number of super-threshold voxels resulting from a threshold of $r^2 = 0.1$. Whereas the average number of super-threshold voxels numerically decreased with age (8.6 k, 8.7 k, 7.9 k, and 7.7 voxels on average for the 30–40, 40–50, 50–60, and 60 + age groups, respectively) no significant differences were found between the age groups or across the APOE groups. Supplementary Fig. S5 provides plots of the number of super-threshold voxels across multiple r^2 thresholds and also density estimates of r^2 distributions for the AGE/APOE sub-groups. Fig. 6 shows a graphical representation of how the breath-hold response features change across different voxel selection threshold. Although the numerical values of specific parameter estimates, and hence also the statistical tests, change with r^2 threshold, the analysis clearly demonstrates that the features are well-behaved across the multiple thresholds and change smoothly without abrupt changes in numerical values or the rankings of the features across the age/APOE sub-groups.

3.4. Analysis of visual stimulation response features

3.4.1. Dependent variables: cosine delay and magnitude

Cosine delay significantly increased with CO_2 with a mean effect of 0.08 s/mmHg ($p = 3.9E-7$). Cosine magnitude significantly decreased with CO_2 level with a mean effect of -0.02%/mmHg ($p = .0073$), whereas no significant associations were found between cosine magnitude and the age, treatment, and APOE factors or the sex and session covariates, respectively (p value associated with the age group factor slightly above the criteria for a significant relation $p = .061$).

3.4.2. Dependent variables: peak time, peak magnitude, and peak width

Peak time significantly increased with CO_2 with a mean effect of 0.08 s/mmHg ($p = 1.3E-6$). Model reduction lead to a final model with the AGE factor and the CO_2 covariate remaining when fitting the peak magnitude (model $p = .0058$). Peak magnitude decreased significantly with age ($p = .019$), Fig. 7D, with a significant decrease when comparing the 30–40 and 50–60 age groups of 0.38% ($p = .033$). Peak magnitude decreased with CO_2 with a mean effect of -0.02%/mmHg ($p = .030$). No significant associations were observed between peak width and any of the experimental factors or the covariates.

3.4.3. Dependence of voxel selection threshold

The number of super-threshold voxels (350, 277, 272, and 184 voxels on average for the 30–40, 40–50, 50–60, and 60 + age groups, respectively) decreased significantly with age (model $p = .024$) with a significant decrease between the 30–40 age group and the 60 + age group ($p = 9.7E-4$), whereas no significant differences were observed between the APOE groups. Supplementary Fig. S6 provide plots of the number of super-threshold voxels versus the r^2 threshold and density

estimates of r^2 distributions for the individual sub-groups. Fig. 8 shows a graphical representation of how the visual stimulation features change across different voxel selection thresholds. The response features appear well behaved in the sense that feature estimates change smoothly as voxel selection thresholds increase, without abrupt changes in the relative estimate sizes or ordering.

4. Discussion

4.1. Study findings

The aim of our present study was to characterize hemodynamic responses, as measured by BOLD fMRI, across the adult age span for subjects with two common APOE genotypes; carriers of the high AD risk e4 allele and non-carrier (e3 homozygotes). Further, we investigated the extent to which these responses were modulated by a short period of increased nitrate ingestion.

Our main finding is that hemodynamic responses to a breath-hold task differ between carriers of the e4 AD risk gene and non-carriers (e3 carrier controls). Middle-aged (50–60 years of age) APOE e4 carriers exhibited a significantly longer peak time relative to middle-aged e3 carriers, while peak time for younger (30–40 years of age) e4 carriers was significantly shorter than that of middle-aged e4 carriers. Overall, peak magnitude significantly decreased with age. Numerically, e4 carriers had reduced peak magnitude, but this effect did not reach our criteria for significance. Nevertheless, the observation of reduced magnitude is consistent with recent reports of reduced hippocampal and whole-brain CO_2 reactivity in younger (20–40 years of age) e4 carriers compared to e3 carriers (Suri et al., 2015). Finally, the response width was consistently and significantly increased in e4 carriers. To our knowledge, our study is the first to quantify changes in timing and the shape of cerebrovascular reactivity responses across APOE allele types in participants without cognitive impairments. A study of cerebrovascular reactivity to CO_2 inhalation in old adults (sub-group mean age between 64 and 72 years of age) has showed decreased BOLD response curve magnitudes in patients diagnosed with MCI or AD relative to controls as well as decreased up-slope gradient of the response curve in AD subjects (Cantin et al., 2011).

In the visual stimulation task, we observed a decreased response magnitude with age. Furthermore, the number of super threshold voxels significantly decreased with age. We did not find any significant influence of APOE genotype on the hemodynamic responses to the visual stimulation task. Our observation of a reduced number of super threshold voxels and a reduced response magnitude with age is in agreement with previous investigations of age-related changes in hemodynamic responses to visual stimulation (Buckner et al., 2000; Ross
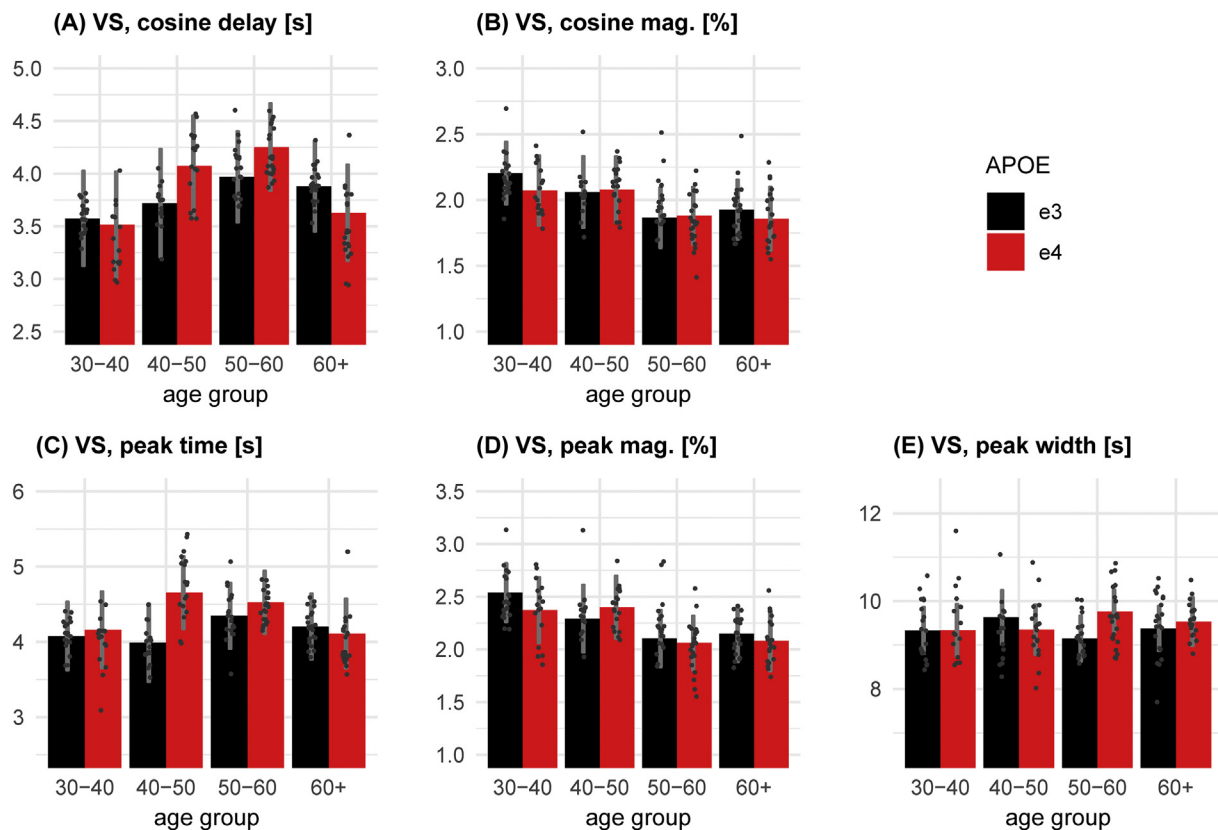
Fig. 7. Visual stimulation response features of BOLD responses estimated across gray matter voxels within the occipital region (voxels with $r^2 > 0.1$. included). Peak magnitude significantly decreased with age. See Section 3.4 for a detailed description of between-group differences. Same format as Fig. 4(A–C).

et al., 1997; Tekes et al., 2005).

We found no significant effects of nitrate ingestion on our hemodynamic response features. We previously demonstrated, that a 3-day period of increased nitrate ingestion alters the hemodynamic response to visual stimulation, reducing response delay and attenuating response magnitude (Aamand et al., 2013). The two studies differ in several aspects i) the study cohort of the previous study was chosen in order to minimize the variations within that study group (20 male participants, 25 ± 0.9 years of age, 77 ± 1.5 kg body weight), ii) image acquisition in the previous study aimed to study visual cortex at a sub-millimeter scale, and iii) the previous fMRI sequence lasted longer (26 min) and applied a different stimulation protocol to allow for repeated estimates of hemodynamics response features. As expected, we observed that increased dietary nitrate over a 3-day ingestion period significantly increased plasma nitrate and nitrite. The daily amount of nitrate given (0.1 mmol per kg body weight per day) is within the range of typical doses used in previous human studies (Lidder and Webb, 2013; Stanaway et al., 2017). With this dose administered over 3 days (and even as a single dose) physiological effects has been observed in several organ systems including effects on blood pressure (Larsen et al., 2006), exercise performance (Larsen et al., 2011), brain perfusion (Presley et al., 2011), and BOLD responses to visual stimulation (Aamand et al., 2013). In our present study cohort, we found a significant reduction in systolic blood pressure with increases nitrate intake. Previous studies have reported mixed results with regard to the influence of dietary nitrate on blood pressure metrics (Stanaway et al., 2017), which may suggest that dietary nitrate has no trivial influence on blood pressure, but its effect instead depends on the individual subject's physiological status. We found no significant influence of increased nitrate intake on heart rate, or transcutaneous recordings of oxygen saturation and CO_2. These findings are in agreement with our previous findings in younger subjects, who underwent an identical nitrate ingestion schedule

(Aamand et al., 2013). At present, there is a limited body of literature on the influence of dietary nitrate on brain hemodynamic metrics. A high nitrate diet has been shown to evoke increased CBF in localized subcortical and deep white matter regions of the frontal lobe but no global CBF changes in older adults (Presley et al., 2011). A study in young adults by near-infrared spectroscopy recordings during cognitive tasks showed no main effect of nitrate ingestion level on the hemodynamic metrics (total hemoglobin and deoxyhemoglobin) (Wightman et al., 2015). Instead, a more advanced pattern was observed, where the extent to which dietary nitrate modulated total hemoglobin recordings depended on the type of cognitive task as well as experimental epoch/ time.

We found a consistent and significant association between average transcutaneous CO_2 measurements and hemodynamic responses features in both the breath-hold task and the visual stimulation task. When interpreting the association between the average transcutaneous CO_2 measurements and the hemodynamic responses features it should be noted that this average CO_2 level may be influenced the relative magnitude of CO_2 increases during breath-hold periods. In both tasks, increased average CO_2 level was associated with increased peak time or delay and decreased response magnitude. Furthermore, the width of the breath-hold response increased with CO_2 level. These results are in agreement with studies investigating the effect of basal CO_2 levels on BOLD responses (Cohen et al., 2002; Stefanovic et al., 2006; van Niftrik et al., 2018). Increasing subjects' basal CBF by CO_2 inhalation has been shown to attenuate BOLD signal changes to functional activation (Stefanovic et al., 2006), and an elevated preset isocapnic baseline has been shown to reduce both cerebrovascular reactivity responses to CO_2 inhalation as well as responses to functional activation (van Niftrik et al., 2018). Changes in basal CBF by hyperventilation and hypercapnia has also been shown not only to modulate the magnitude of BOLD responses to visual stimulation but also to alter the temporal
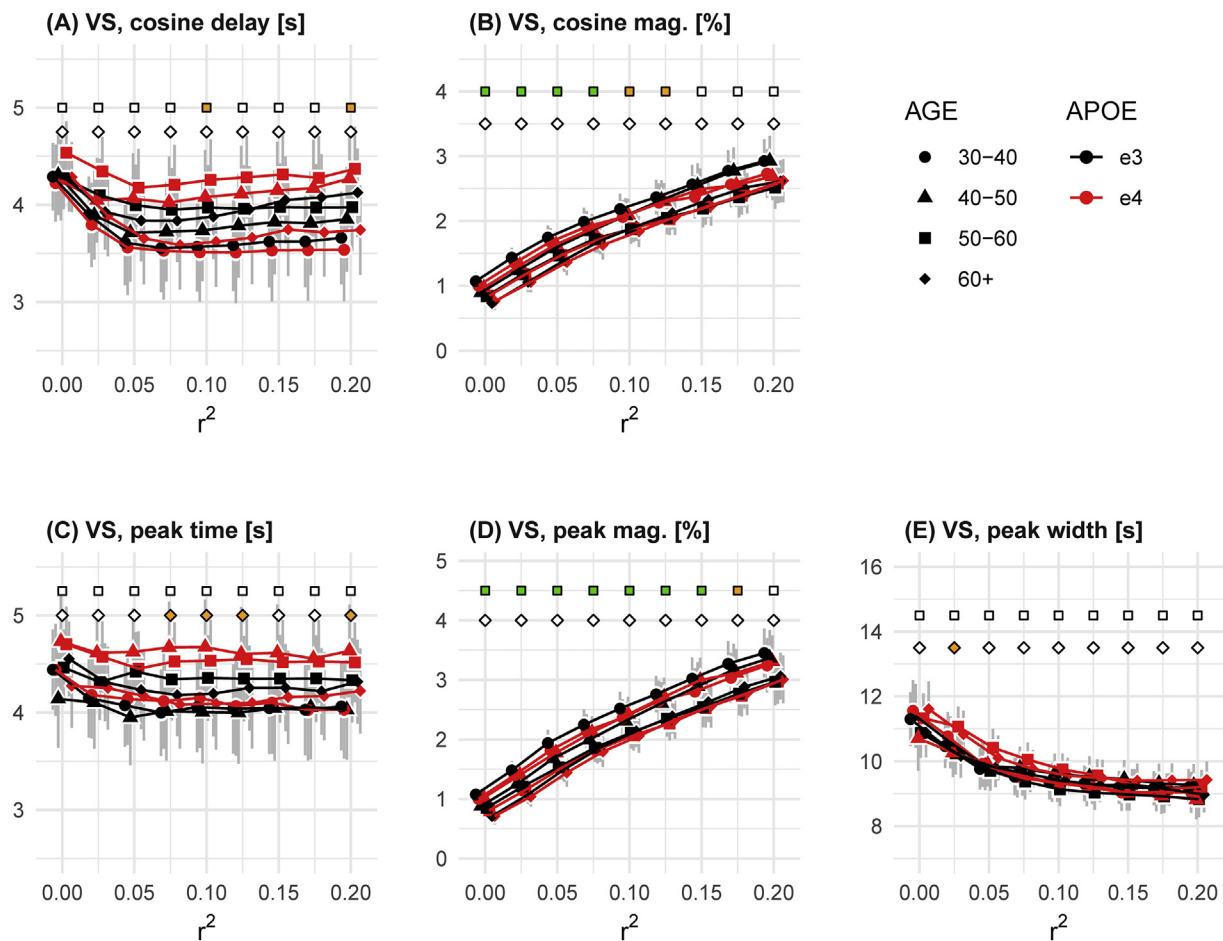
Fig. 8. Dependence of voxel selection threshold (r^2) on visual stimulation response features. Same format as Fig. 4(D–F).

dynamics of these response curves, with peak magnitude decreased with increased CO_2 level and peak time and response width both increasing with increased CO_2 level (Cohen et al., 2002). We note, that differences in basal CO_2 level across our AGE/APOE sub-groups are not likely to cause the significant between-group differences in our hemodynamic response features since (i) no significant differences in CO_2 level was observed across the sub-groups, and (ii) CO_2 level was included as a covariate in the linear mixed model analysis of the hemodynamic response features. Hence, the CO_2 level accounted for a significant part of the between-subject variability rather than between-group variability.

4.2. Physiological interpretation

Assessment of cerebrovascular reactivity provides a means for probing the regulation and distribution of blood flow across brain tissue (Fierstra et al., 2013). Technically, cerebrovascular reactivity quantifies the vascular response to a vasoactive stimulus signal, and perturbations in the blood content of CO_2 is a frequently used stimulus in functional neuroimaging contexts. Increases in blood CO_2 levels result in relaxation of VSMCs and concomitant increases in CBF (Ainslie and Duffin, 2009). Whereas active signaling mechanisms has been implicated in the reactivity response to CO_2 (Ainslie and Duffin, 2009; Howarth et al., 2017) passive mechanisms, for example downstream passive dilation due to changes in blood pressure, may also be accountable for part of the response (Ainslie and Duffin, 2009). Inhibition of NOS has been shown to attenuate CBF responses to hypercapnia in experimental models, indicating that the effects of CO_2 on the cerebral circulation is mediated by NO (Iadecola, 1992). In the present study, we used a

breath-hold task to evoke changes in CO_2 levels. Hence, the breath-hold task (paced respiration and 13.5 s of after end-expiration breath-hold) is the experimental quantity that is standardized across participants and scanning sessions. During this standardized period of breath-hold, the elimination of CO_2 from blood is reduced resulting in an accumulation of CO_2 in blood over time. Since this raise in blood CO_2 depends on the individual subject's physiology, for example metabolic rate of oxygen consumption, such influential factors must be remembered when interpreting our findings. Importantly, with regard to key physiological variables we found no significant differences in height, weight, BMI, breathing-rate, pulse rate, and blood pressure across APOE types, suggesting absence of obvious bias sources across APOE types.

Vascular dysfunction has been implicated in the pathogenesis of AD. We found changes in the hemodynamic response to breath-hold in e4 carriers. The BOLD signal is sensitive to the local amount of deoxyhemoglobin, which in turn, depends on oxygen supply as well as oxygen extraction and consumption. Our observations of significantly altered hemodynamic responses in e4 carriers may provide support to the hypothesis of an impaired vascular function in e4 carriers. The pattern of increased response widths in e4 carriers, increased peak times in mid-aged e4 carriers, and reduced peak time in young e4 carriers, may reflect dynamic adjustments of vascular responses to optimize oxygen extraction in response to evolving structural and functional microvascular changes that tend to permit 'shunting' of oxygenated blood through the microvasculature (Østergaard et al., 2013). The pattern of attenuated and more dispersed BOLD responses in e4 carriers may thus be reflective of a microvascular system with impaired ability to support normal oxygen utilization at normal tissue oxygen tension. In particular, we speculate that the breath-hold BOLD

responses may provide a sensitive means of studying changes in microvascular function in healthy ageing and preclinical dementia.

4.3. Methodological consideration and future directions

In our main analysis, we partitioned participants into four age groups defined by decades. The advantage of grouping participants according to their age into a discrete number of groups is the possibility for quantifying age related changes by comparing different age groups by partial tests. In a supplementary analysis, we additionally treated age as a continuous variable (Supplementary Figs. S7–S8). We found consistency between the two analysis strategies (continuous age vs. age groups) and our results are thus robust across the two modeling strategies.

In the present study, we used an experimental paradigm with concurrent breath-hold and visual stimulation tasks (Cohen et al., 2002; Stefanovic et al., 2006). This strategy was chosen to provide hemodynamic characteristics of both cerebrovascular reactivity responses as well as responses to functional activation under the constraint of a limited available scan time of 10 min. The wedge or traveling wave approach to study functional activation was chosen to use scan time efficiently in the sense that visual simulation was present almost throughout the entire acquisition period rather than in limited periods of time as in conventional block paradigms. Different cortical regions are continuously activated at different times by the traveling wave approach, and the corresponding hemodynamic response would therefore be sampled at a wide range of different time points. Indeed, this approach has previously shown to provide a sensitive means for detection of hemodynamic alterations evoked by nitrate ingestion (Aamand et al., 2013). However, one potential limitation of this approach is that voxel-wise response phases need to be estimated in order to achieve an average hemodynamic response by temporally shifting individual voxels' response curves. This, in turn, implies that uncertainties and inaccuracies in phase estimates propagate to uncertainties in the corresponding average hemodynamic response curves. However, our analysis of between-session reproducibility of the response features suggests a relatively high reproducibility of the visual stimulation response features with between-session correlations. Adopting a block sequence for the visual stimulation (Cohen et al., 2002; Stefanovic et al., 2006), as done for the breath-hold task, would alleviate the challenge in pooling the hemodynamic responses across voxels, but this comes with the cost, that a considerable amount of the total scan time is spend without visual stimulation. Another potential limitation to the concurrent breath-hold and visual stimulation tasks is the possible interaction between the two tasks. Breath-hold and paced respiration lead to changes in CO_2 level over time, and changes in CO_2 levels have been shown to impact the dynamics of visually evoked BOLD responses (Cohen et al., 2002). This interaction could lead to heterogeneity in the visually evoked BOLD responses over time, which, in turn, could decrease the sensitivity of the subsequent signal detection and quantification. Whereas the concurrent tasks may influence the detection of visually evoked BOLD responses we do not expect the breath-hold induced BOLD responses to be significantly influenced by this possible interaction since our findings related to breath-hold responses are rather consistent across brain regions. A formal development and evaluation of efficient experimental paradigms for concurrent characterization of cerebrovascular reactivity responses to breath-hold and functional activation-induced responses is an interesting topic that deserves attention in future research.

In addition to the observed between-group differences in peak time, peak magnitude, and peak width we consistently observed a negative "dip" during the breath-hold period across all groups (Fig. 5). Although biphasic responses with a strong initial negative response are observed for breath-holds after inspiration (Kastrup et al., 1998), our finding of a smaller initial dip evoked by breath-hold after expiration is in agreement with previous reports of breath-hold responses after expiration

(Scouten and Schwarzbauer, 2008). CBF responses, measured by flow-sensitive alternating inversion recovery (FAIR), showed a biphasic pattern for breath-hold after inspiration but only a positive response for breath-hold after expiration (Li et al., 1999). To our knowledge, the mechanism underlying the "initial dip" evoked by breath-hold after expiration is yet to be established and is a topic for future research.

We used a breath-hold task to study cerebrovascular reactivity. Breath-holding provides a simple means to evoke cerebrovascular reactivity responses (Kastrup et al., 2001; Kastrup et al., 1999; Urback et al., 2017). To optimize the robustness of the breath-hold stimuli we adopted an experimental strategy with paced breathing and breath-hold after end-expiration, (Bright and Murphy, 2013; Murphy et al., 2011; Scouten and Schwarzbauer, 2008; Urback et al., 2017), and with the breathing rate targeted to match the subject's natural breathing rate (Bright and Murphy, 2013). The length of the breath-hold periods (13.5 s) is within the ranges used in previous studies (Bright and Murphy, 2013) and chosen to ensure that the breath-hold task was well tolerated by the participants with ages spanning the 30–70 years of age interval. A frequently used approach to model breath-hold responses is to use end-tidal CO_2 recordings in linear modeling (Kastrup et al., 2001; Murphy et al., 2011; Scouten and Schwarzbauer, 2008). As compared to alternatives, this approach have two potential strengths. The first strength is that end-tidal CO_2, potentially convolved with hemodynamic response function and temporal derivative included as additional repressor (Murphy et al., 2011), yields a better and more robust fit to breath-hold hold responses than more simple time shifted stimulus blocks or ramps that are convolved with the hemodynamic response function (Bright and Murphy, 2013; Murphy et al., 2011). The second strength is of a biological nature: The breath-hold task elicits hemodynamic responses through a chain of signaling events, that involves a wide range of physiological processes. From one standpoint, the arterial partial pressure of CO_2 is the key vasoactive stimuli to be standardized across subjects (Fierstra et al., 2013). Although a breath-hold task is standardized across subjects within a given study, the actual change in arterial tension of CO_2 vary across subjects (Murphy et al., 2011) depending on individual lung capacities, respiration pattern, and metabolic rates among others (Fierstra et al., 2013). A positive correlation between breath-hold induced signal changes and individual-subject estimates of end-tidal CO_2 changes increase during breath-hold has been observed (Murphy et al., 2011). Normalizing BOLD response changes by end-tidal measures, to yield the unit of [% change/mmHg], provides a means for standardizing the response magnitude (Kastrup et al., 2001), and it has been argued that this strategy renders breath-hold CVR metrics more robust (Murphy et al., 2011). We modeled the breath-hold responses by sine-cosine regressors at the task frequency (including higher order harmonics). The sine-cosine model has been shown to perform on par with modeling based on end-tidal CO_2 recordings, with no significant difference, on average, over the whole brain in variance explained between the two methods (Murphy et al., 2011). We measured CO_2 levels by transcutaneous recordings, and the average recordings were stable across experimental sessions as demonstrated by our reproducibility analysis. However, the temporal response characteristics of the CO_2 sensor did not allow for characterization of changes in CO_2 levels evoked by individual breath-hold epochs and we, hence, used non-normalized percent-changes for the response magnitude metric. Although this strategy may decrease the analysis sensitivity because of increased between-subject variance, it is important to note, that the conventional normalization according to end-tidal CO_2 changes is a global normalization. Therefore, only the results regarding our response magnitude feature would potentially be affected by this normalization. On the other hand, the peak time and response width features are invariant to such global normalization, and these features and corresponding analysis results would be unaffected by normalization. An interesting topic for future research is to evoke reactivity responses by use a controllable gas delivery device instead of breath-holding (Fierstra et al., 2013), and to study the temporal

characteristics of these in a study cohort similar to our present cohort.

5. Conclusions

We found that the BOLD response to the breath-hold task was altered in APOE e4 carriers relative to e3 carriers. Mid-aged (50–60 years of age) e4 carriers exhibited a significantly increased peak time relative to mid-aged e3 carriers, and peak time for younger (30–40 years of age) e4 carriers was significantly shorter than that of mid-aged e4 carriers. The response width was consistently and significantly increased for e4 carriers. Overall, peak magnitude significantly decreased with age. These effects were present both in a gray matter ROI, and in smaller ROI's based on either anatomical or resting state atlases. For the visual stimulation task we found age-related decreases in the BOLD signal, with reduced response magnitude with age but no significant effect of APOE allele type. We found no effect of increased nitrate ingestion on the BOLD responses evoked by the breath-hold or visual stimulation tasks.

Funding and acknowledgements

Declarations of interest

None.

Appendix A. Supplementary data

Supplementary data to this article can be found online at https://doi.org/10.1016/j.nicl.2019.101955.

References

Aamand, R., Dalsgaard, T., Ho, Y.C., Moller, A., Roepstorff, A., Lund, T.E., 2013. A NO way to BOLD? Dietary nitrate alters the hemodynamic response to visual stimulation. Neuroimage 83, 397–407.
Ainslie, P.N., Duffin, J., 2009. Integration of cerebrovascular CO2 reactivity and chemoreflex control of breathing: mechanisms of regulation, measurement, and interpretation. Am. J. Phys. Regul. Integr. Comp. Phys. 296, R1473–R1495.
Aizenstein, H.J., Clark, K.A., Butters, M.A., Cochran, J., Stenger, V.A., Meltzer, C.C., Reynolds, C.F., Carter, C.S., 2004. The BOLD hemodynamic response in healthy aging. J. Cogn. Neurosci. 16, 786–793.
Albrecht, E.W., Stegeman, C.A., Heeringa, P., Henning, R.H., van Goor, H., 2003. Protective role of endothelial nitric oxide synthase. J. Pathol. 199, 8–17.
Alzheimer's Association, 2018. 2018 Alzheimer's disease facts and figures. Alzheimers Dementi. J. Alzheimer Assoc. 14, 367–429.
Ances, B.M., Liang, C.L., Leontiev, O., Perthen, J.E., Fleisher, A.S., Lansing, A.E., Buxton, R.B., 2009. Effects of aging on cerebral blood flow, oxygen metabolism, and blood oxygenation level dependent responses to visual stimulation. Hum. Brain Mapp. 30, 1120–1132.
Attwell, D., Buchan, A.M., Charpak, S., Lauritzen, M., Macvicar, B.A., Newman, E.A., 2010. Glial and neuronal control of brain blood flow. Nature 468, 232–243.
Bates, D., Machler, M., Bolker, B.M., Walker, S.C., 2015. Fitting linear mixed-effects models using lme4. J. Stat. Softw. 67, 1–48.
Bondonno, C.P., Croft, K.D., Hodgson, J.M., 2016. Dietary nitrate, nitric oxide, and cardiovascular health. Crit. Rev. Food Sci. Nutr. 56, 2036–2052.
Bright, M.G., Murphy, K., 2013. Reliable quantification of BOLD fMRI cerebrovascular reactivity despite poor breath-hold performance. Neuroimage 83, 559–568.
Buckner, R.L., Snyder, A.Z., Sanders, A.L., Raichle, M.E., Morris, J.C., 2000. Functional brain imaging of young, nondemented, and demented older adults. J. Cogn. Neurosci. 12 (Suppl. 2), 24–34.
Cantin, S., Villien, M., Moreaud, O., Tropres, I., Keignart, S., Chipon, E., Le Bas, J.F., Warnking, J., Krainik, A., 2011. Impaired cerebral vasoreactivity to CO2 in Alzheimer's disease using BOLD fMRI. Neuroimage 58, 579–587.
Cohen, E.R., Ugurbil, K., Kim, S.G., 2002. Effect of basal conditions on the magnitude and dynamics of the blood oxygenation level-dependent fMRI response. J. Cereb. Blood Flow Metab. 22, 1042–1053.
de la Torre, J.C., 2004. Is Alzheimer's disease a neurodegenerative or a vascular disorder?

Data, dogma, and dialectics. Lancet Neurol. 3, 184–190.
de la Torre, J.C., Stefano, G.B., 2000. Evidence that Alzheimer's disease is a microvascular disorder: the role of constitutive nitric oxide. Brain Res. Brain Res. Rev. 34, 119–136.
D'Esposito, M., Zarahn, E., Aguirre, G.K., Rypma, B., 1999. The effect of normal aging on the coupling of neural activity to the bold hemodynamic response. Neuroimage 10, 6–14.
D'Esposito, M., Deouell, L.Y., Gazzaley, A., 2003. Alterations in the BOLD fMRI signal with ageing and disease: a challenge for neuroimaging. Nat. Rev. Neurosci. 4, 863–872.
Farkas, E., Luiten, P.G., 2001. Cerebral microvascular pathology in aging and Alzheimer's disease. Prog. Neurobiol. 64, 575–611.
Fierstra, J., Sobczyk, O., Battisti-Charbonney, A., Mandell, D.M., Poublanc, J., Crawley, A.P., Mikulis, D.J., Duffin, J., Fisher, J.A., 2013. Measuring cerebrovascular reactivity: what stimulus to use? J. Physiol. 591, 5809–5821.
Fleisher, A.S., Podraza, K.M., Bangen, K.J., Taylor, C., Sherzai, A., Sidhar, K., Liu, T.T., Dale, A.M., Buxton, R.B., 2009. Cerebral perfusion and oxygenation differences in Alzheimer's disease risk. Neurobiol. Aging 21, 1737–1748.
Glover, G.H., Li, T.Q., Ress, D., 2000. Image-based method for retrospective correction of physiological motion effects in fMRI: RETROICOR. Magn. Reson. Med. 44, 162–167.
Hajjar, I., Sorond, F., Lipsitz, L.A., 2015. Apolipoprotein E, carbon dioxide vasoreactivity, and cognition in older adults: effect of hypertension. J. Am. Geriatr. Soc. 63, 276–281.
Halekoh, U., Højsgaard, S., 2014. A Kenward-Roger approximation and parametric bootstrap methods for tests in linear mixed models. R Packag. pbkrtest 59, 32.
Hesselmann, V., Zaro Weber, O., Wedekind, C., Krings, T., Schulte, O., Kugel, H., Krug, B., Klug, N., Lackner, K.J., 2001. Age related signal decrease in functional magnetic resonance imaging during motor stimulation in humans. Neurosci. Lett. 308, 141–144.
Howarth, C., Sutherland, B., Choi, H.B., Martin, C., Lind, B.L., Khennouf, L., LeDue, J.M., Pakan, J.M., Ko, R.W., Ellis-Davies, G., Lauritzen, M., Sibson, N.R., Buchan, A.M., MacVicar, B.A., 2017. A critical role for astrocytes in hypercapnic vasodilation in brain. J. Neurosci. 37, 2403–2414.
Huettel, S.A., Singerman, J.D., McCarthy, G., 2001. The effects of aging upon the hemodynamic response measured by functional MRI. Neuroimage 13, 161–175.
Iadecola, C., 1992. Does nitric-oxide mediate the increases in cerebral blood-flow elicited by hypercapnia. Proc. Natl. Acad. Sci. U. S. A. 89, 3913–3916.
Iadecola, C., 2004. Neurovascular regulation in the normal brain and in Alzheimer's disease. Nat. Rev. Neurosci. 5, 347–360.
Iadecola, C., 2017. The neurovascular unit coming of age: a journey through neurovascular coupling in health and disease. Neuron 96, 17–42.
Ito, H., Kanno, I., Ibaraki, M., Hatazawa, J., 2002. Effect of aging on cerebral vascular response to paco2 changes in humans as measured by positron emission tomography. J. Cereb. Blood Flow Metab. 22, 997–1003.
Jespersen, S.N., Østergaard, L., 2012. The roles of cerebral blood flow, capillary transit time heterogeneity, and oxygen tension in brain oxygenation and metabolism. J. Cereb. Blood Flow Metab. 32, 264–277.
Kastrup, A., Li, T.Q., Takahashi, A., Glover, G.H., Moseley, M.E., 1998. Functional magnetic resonance imaging of regional cerebral blood oxygenation changes during breath holding. Stroke 29, 2641–2645.
Kastrup, A., Li, T.Q., Glover, G.H., Moseley, M.E., 1999. Cerebral blood flow-related signal changes during breath-holding. AJNR Am. J. Neuroradiol. 20, 1233–1238.
Kastrup, A., Kruger, G., Neumann-Haefelin, T., Moseley, M.E., 2001. Assessment of cerebrovascular reactivity with functional magnetic resonance imaging: comparison of CO(2) and breath holding. Magn. Reson. Imaging 19, 13–20.
Katusic, Z.S., Austin, S.A., 2014. Endothelial nitric oxide: protector of a healthy mind. Eur. Heart J. 35, 888–894.
Kisler, K., Nelson, A.R., Montagne, A., Zlokovic, B.V., 2017. Cerebral blood flow regulation and neurovascular dysfunction in Alzheimer disease. Nat. Rev. Neurosci. 18, 419–434.
Kuznetsova, A., Brockhoff, P.B., Christensen, R.H.B., 2017. lmerTest package: tests in linear mixed effects models. J. Stat. Softw. 82, 1–26.
Larsen, F.J., Ekblom, B., Sahlin, K., Lundberg, J.O., Weitzberg, E., 2006. Effects of dietary nitrate on blood pressure in healthy volunteers. N. Engl. J. Med. 355, 2792–2793.
Larsen, F.J., Schiffer, T.A., Borniquel, S., Sahlin, K., Ekblom, B., Lundberg, J.O., Weitzberg, E., 2011. Dietary inorganic nitrate improves mitochondrial efficiency in humans. Cell Metab. 13, 149–159.
Lavi, S., Egbarya, R., Lavi, R., Jacob, G., 2003. Role of nitric oxide in the regulation of cerebral blood flow in humans: chemoregulation versus mechanoregulation. Circulation 107, 1901–1905.
Lavi, S., Gaitini, D., Milloul, V., Jacob, G., 2006. Impaired cerebral CO2 vasoreactivity: association with endothelial dysfunction. Am. J. Physiol. Heart Circ. Physiol. 291, H1856–H1861.
Li, T.Q., Kastrup, A., Takahashi, A.M., Moseley, M.E., 1999. Functional MRI of human brain during breath holding by BOLD and FAIR techniques. Neuroimage 9, 243–249.
Lidder, S., Webb, A.J., 2013. Vascular effects of dietary nitrate (as found in green leafy vegetables and beetroot) via the nitrate-nitrite-nitric oxide pathway. Br. J. Clin. Pharmacol. 75, 677–696.
Lu, H., Xu, F., Rodrigue, K.M., Kennedy, K.M., Cheng, Y., Flicker, B., Hebrank, A.C., Uh, J., Park, D.C., 2011. Alterations in cerebral metabolic rate and blood supply across the adult lifespan. Cereb. Cortex 21, 1426–1434.
Lund, T.E., Madsen, K.H., Sidaros, K., Luo, W.L., Nichols, T.E., 2006. Non-white noise in fMRI: does modelling have an impact? Neuroimage 29, 54–66.
Lundberg, J.O., Weitzberg, E., Gladwin, M.T., 2008. The nitrate-nitrite-nitric oxide pathway in physiology and therapeutics. Nat. Rev. Drug Discov. 7, 156–167.
Murphy, K., Harris, A.D., Wise, R.G., 2011. Robustly measuring vascular reactivity differences with breath-hold: normalising stimulus-evoked and resting state BOLD fMRI

data. Neuroimage 54, 369–379.

Nelson, A.R., Sweeney, M.D., Sagare, A.P., Zlokovic, B.V., 2016. Neurovascular dysfunction and neurodegeneration in dementia and Alzheimer's disease. Biochim. Biophys. Acta 1862, 887–900.

Niwa, K., Younkin, L., Ebeling, C., Turner, S.K., Westaway, D., Younkin, S., Ashe, K.H., Carlson, G.A., Iadecola, C., 2000. Abeta 1-40-related reduction in functional hyperemia in mouse neocortex during somatosensory activation. Proc. Natl. Acad. Sci. U. S. A. 97, 9735–9740.

Østergaard, L., Aamand, R., Gutierrez-Jimenez, E., Ho, Y.C., Blicher, J.U., Madsen, S.M., Nagenthiraja, K., Dalby, R.B., Drasbek, K.R., Moller, A., Braendgaard, H., Mouridsen, K., Jespersen, S.N., Jensen, M.S., West, M.J., 2013. The capillary dysfunction hypothesis of Alzheimer's disease. Neurobiol. Aging 34, 1018–1031.

Peng, S.L., Chen, X., Li, Y., Rodrigue, K.M., Park, D.C., Lu, H., 2018. Age-related changes in cerebrovascular reactivity and their relationship to cognition: a four-year longitudinal study. Neuroimage 174, 257–262.

Presley, T.D., Morgan, A.R., Bechtold, E., Clodfelter, W., Dove, R.W., Jennings, J.M., Kraft, R.A., King, S.B., Laurienti, P.J., Rejeski, W.J., Burdette, J.H., Kim-Shapiro, D.B., Miller, G.D., 2011. Acute effect of a high nitrate diet on brain perfusion in older adults. Nitric Oxide 24, 34–42.

Raut, R.V., Nair, V.A., Sattin, J.A., Prabhakaran, V., 2016. Hypercapnic evaluation of vascular reactivity in healthy aging and acute stroke via functional MRI. Neuroimage Clin. 12, 173–179.

Reich, T., Rusinek, H., 1989. Cerebral cortical and white matter reactivity to carbon dioxide. Stroke 20, 453–457.

Ross, M.H., Yurgelun-Todd, D.A., Renshaw, P.F., Maas, L.C., Mendelson, J.H., Mello, N.K., Cohen, B.M., Levin, J.M., 1997. Age-related reduction in functional MRI response to photic stimulation. Neurology 48, 173–176.

Scarmeas, N., Habeck, C.G., Hilton, J., Anderson, K.E., Flynn, J., Park, A., Stern, Y., 2005. APOE related alterations in cerebral activation even at college age. J. Neurol. Neurosurg. Psychiatry 76, 1440–1444.

Schmetterer, L., Findl, O., Strenn, K., Graselli, U., Kastner, J., Eichler, H.G., Wolzt, M., 1997. Role of NO in the O2 and CO2 responsiveness of cerebral and ocular circulation in humans. Am. J. Phys. 273, R2005–R2012.

Scouten, A., Schwarzbauer, C., 2008. Paced respiration with end-expiration technique offers superior BOLD signal repeatability for breath-hold studies. Neuroimage 43,

250–257.

Stanaway, L., Rutherfurd-Markwick, K., Page, R., Ali, A., 2017. Performance and health benefits of dietary nitrate supplementation in older adults: a systematic review. Nutrients 9.

Stefanovic, B., Warnking, J.M., Rylander, K.M., Pike, G.B., 2006. The effect of global cerebral vasodilation on focal activation hemodynamics. Neuroimage 30, 726–734.

Suri, S., Mackay, C.E., Kelly, M.E., Germuska, M., Tunbridge, E.M., Frisoni, G.B., Matthews, P.M., Ebmeier, K.P., Bulte, D.P., Filippini, N., 2015. Reduced cerebrovascular reactivity in young adults carrying the APOE epsilon4 allele. Alzheimers Dement. 11 (648-657), e641.

Team, R.D.C., 2010. R: A Language and Environment for Statistical Computing. R Foundation for Statistical Computing, Vienna, Austria.

Tekes, A., Mohamed, M.A., Browner, N.M., Calhoun, V.D., Yousem, D.M., 2005. Effect of age on visuomotor functional MR imaging. Acad. Radiol. 12, 739–745.

Thambisetty, M., Beason-Held, L., An, Y., Kraut, M.A., Resnick, S.M., 2010. APOE epsilon4 genotype and longitudinal changes in cerebral blood flow in normal aging. Arch. Neurol. 67, 93–98.

Thirion, B., Duchesnay, E., Hubbard, E., Dubois, J., Poline, J.B., Lebihan, D., Dehaene, S., 2006. Inverse retinotopy: inferring the visual content of images from brain activation patterns. Neuroimage 33, 1104–1116.

Trachtenberg, A.J., Filippini, N., Mackay, C.E., 2012. The effects of APOE-epsilon4 on the BOLD response. Neurobiol. Aging 33, 323–334.

Urback, A.L., MacIntosh, B.J., Goldstein, B.I., 2017. Cerebrovascular reactivity measured by functional magnetic resonance imaging during breath-hold challenge: a systematic review. Neurosci. Biobehav. Rev. 79, 27–47.

van Niftrik, C.H.B., Piccirelli, M., Bozinov, O., Maldaner, N., Strittmatter, C., Pangalu, A., Valavanis, A., Regli, L., Fierstra, J., 2018. Impact of baseline CO2 on blood-oxygenation-level-dependent MRI measurements of cerebrovascular reactivity and task-evoked signal activation. Magn. Reson. Imaging 49, 123–130.

Whitfield-Gabrieli, S., Nieto-Castanon, A., 2012. Conn: a functional connectivity toolbox for correlated and anticorrelated brain networks. Brain Connect 2, 125–141.

Wightman, E.L., Haskell-Ramsay, C.F., Thompson, K.G., Blackwell, J.R., Winyard, P.G., Forster, J., Jones, A.M., Kennedy, D.O., 2015. Dietary nitrate modulates cerebral blood flow parameters and cognitive performance in humans: a double-blind, placebo-controlled, crossover investigation. Physiol. Behav. 149, 149–158.